

4
5
6
7
8
9
10
11
12
13
14
15
16
17
18
19
20
21
22
23
24
25
26
27
28
29
30
31
32
33
34
35
36
37
38
39
40
41
42
43
44
45
46
47
48
49
50
51
52
53
54
55
56
57
58
59
60
61
62
63
64
65

Photoreceptor Damage and Foveal Sensitivity in Surgically Closed Macular Holes: An Adaptive Optics Scanning Laser Ophthalmoscopy Study

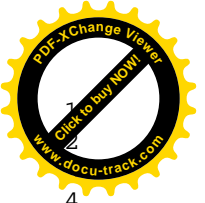
Short Title: Photoreceptor damage and sensitivity in closed macular hole

SOTARO OOTO, MASANORI HANGAI, KOHEI TAKAYAMA, NAOKO UEDA-
ARAKAWA, MASA AKI HANEBUCHI, AND NAGAHISA YOSHIMURA

From the Department of Ophthalmology and Visual Sciences, Kyoto University Graduate School of Medicine, Kyoto, Japan (S.O., M.Hangai, K.T., N.U.A.,N.Y.) and NIDEK Co., Ltd, Gamagori, Japan (M.Hanubuchi)

Supplemental Material available at AJO.com.

Inquiries to Sotaro Ooto, Assistant Professor, Department of Ophthalmology and Visual Sciences, Kyoto University Graduate School of Medicine, 54 Kawahara-cho, Shogoin, Sakyo-ku, Kyoto 606-8507, Japan;
Telephone: +81-75-751-3248; Fax: +81-75-752-0933
E-mail: ohoto@kuhp.kyoto-u.ac.jp



4
5
6
7
8
9
10
11
12
13
14
15
16
17
18
19
20
21
22
23
24
25
26
27
28
29
30
31
32
33
34
35
36
37
38
39
40
41
42
43
44
45
46
47
48
49
50
51
52
53
54
55
56
57
58
59
60
61
62
63
64
65

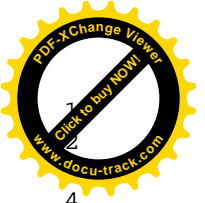
INTRODUCTION

Idiopathic macular hole (MH) generally occurs in otherwise healthy individuals, is more common in women, and usually decreases previously normal visual acuity to less than 20/100. MH can be closed successfully with vitreoretinal surgical techniques,¹⁻³ but complete anatomic closure does not always result in satisfactory recovery of visual acuity. In addition, some patients with closed MH continue to have symptoms such as relative scotoma and metamorphopsia.⁴⁻⁶

Optical coherence tomography (OCT) has become the gold standard for the diagnosis of MH and for confirming anatomic closure after surgery. Structural changes in the photoreceptor layers of eyes with surgically closed MH, such as varying degrees of disruption of the junction between the photoreceptor inner and outer segments (IS/OS) and of the external limiting membrane (ELM), have been identified using time-domain OCT (TD-OCT),⁷⁻¹⁷ ultrahigh-resolution OCT,^{18,19} and spectral-domain OCT (SD-OCT).²⁰⁻²⁷ These imaging modalities have not, however, provided sufficiently clear images of individual photoreceptor cells to allow identification of a specific structural abnormality that might explain persistent visual disturbance in eyes with closed MH.

The primary reason for this failure is that ocular optics possess aberrations, which can be compensated for by incorporating adaptive optics (AO)—specifically, either OCT or another imaging technique such as scanning laser ophthalmoscopy (SLO)—into the imaging system. An AO system consists of a wavefront sensor that measures aberrations of the whole eye, and a deformable mirror or a spatial light modulator that compensates for these aberrations in living eyes.²⁸⁻³² The addition of AO to imaging systems such as flood-illuminated ophthalmoscopes or SLO equipment has allowed researchers to obtain clear images of microstructural details in living eyes, including abnormalities in individual cone photoreceptors in patients with various retinal diseases.³³⁻⁴⁴

In the current study, we used the AO-SLO system to investigate relationships between structural abnormalities (decreased cone density and areas of cone loss) and visual function (foveal sensitivity, as measured by microperimetry and visual acuity) after surgical closure of MH, as well as relationships between structural abnormalities before and after surgery.



4
5
6
7
8
9
10
11
12
13
14
15
16
17
18
19
20
21
22
23
24
25
26
27
28
29
30
31
32
33
34
35
36
37
38
39
40
41
42
43
44
45
46
47
48
49
50
51
52
53
54
55
56
57
58
59
60
61
62
63
64
65

METHODS

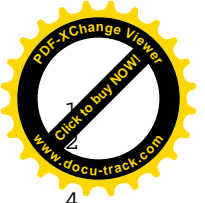
Participants

There were a total of 34 participants in this prospective interventional case study. Nineteen were patients (21 eyes; 6 men and 13 women; mean age: 67.5 years, range: 55-82) with idiopathic MH but without any other macular abnormality, glaucoma, or inherited color blindness; all patients visited the Kyoto University Hospital, Kyoto, Japan, between February 2010 and October 2010. The other 15 participants were healthy volunteers (15 eyes; 5 men and 10 women, mean age: 61.2 years, range: 35-72) with no eye diseases.

All patients had a diagnosis of primary stage 2, 3, or 4 idiopathic MH according to the staging system proposed by Gass;⁴⁵ we excluded eyes with secondary MH (e.g., due to trauma, occurring after laser treatment, or due to cystoid macular edema resulting from inflammation, retinal vascular disease, macular pucker, or retinal detachment). We also excluded eyes with high myopia (axial length > 26.5 mm). Finally, we excluded from the final study data analysis 1 eye of a study patient in which foveal detachment^{15,16,25} was diagnosed at the 6-month postoperative visit, since this condition precluded our evaluation of photoreceptors via AO-SLO imaging.

Ophthalmologic Examinations

All patients in this study underwent comprehensive ophthalmologic examinations at baseline and 6 months after surgical closure of MH. The following characteristics were measured during baseline evaluations: best-corrected visual acuity (BCVA), assessed with the Landolt chart and expressed as the logarithm of the minimal angle of resolution (logMAR); intraocular pressure (IOP); and axial length, assessed using an IOL Master (Carl Zeiss Meditec, Dublin, CA, USA). At the baseline, we also performed indirect ophthalmoscopy, slit-lamp biomicroscopy with a contact lens, color fundus photography, and SD-OCT. At the 6-month postoperative evaluation, we measured BCVA and performed indirect ophthalmoscopy, slit-lamp biomicroscopy with a contact lens, color fundus photography, SD-OCT, AO-SLO, and fundus-monitoring microperimetry (MP; MP-1, NIDEK, Padova, Italy).



4
5
6
7
8
9
10
11
12
13
14
15
16
17
18
19
20
21
22
23
24
25
26
27
28
29
30
31
32
33
34
35
36
37
38
39
40
41
42
43
44
45
46
47
48
49
50
51
52
53
54
55
56
57
58
59
60
61
62
63
64
65

All volunteers underwent a comprehensive ophthalmologic examination, including measurements of BCVA, IOP, and axial length, indirect ophthalmoscopy, color fundus photography, SD-OCT, AO-SLO, and MP.

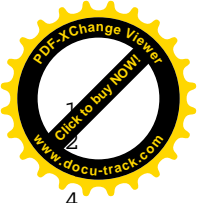
The Adaptive Optics Scanning Laser Ophthalmoscopy System

The AO-SLO system used here was a simplified version designed and constructed in our laboratory⁴²⁻⁴⁴ based on previous reports detailing the usefulness of incorporating a wide-field SLO with an AO-SLO.^{46,47} The AO-SLO system is confocal, enabling creation of high-contrast “en face” images in any plane; these images show individual cone photoreceptor cells. The system is composed of 4 primary optical subsystems: the AO subsystem, which includes the wavefront sensor and the spatial light modulator; the high-resolution confocal SLO imaging subsystem; the wide-field imaging subsystem; and the pupil observation subsystem, which facilitates the initial alignment of the subject’s pupil with respect to the optical axis of the AO-SLO system through adjustment of the chin rest position. The wavefront sensor measures aberrations in the whole eye, and the spatial light modulator compensates for these aberrations. The details of the AO-SLO system are described in the Supplemental Material. (Supplemental Material at AJO.com)

Adaptive Optics Scanning Laser Ophthalmoscopy Imaging of Cone Mosaic Features

For each eye, we acquired a series of AO-SLO images at each of several locations in the macula. The series at each location was acquired by shifting the focus from the retinal nerve fiber layer (RNFL) to the retinal pigmented epithelium (RPE), with particular attention being paid to acquisition of images that showed the cone mosaic. Then, offline, we created a montage of AO-SLO images for each eye by selecting the area of interest and generating each image to be included in the montage from a single frame, without averaging. We verified correspondence between each montage and the area of interest by comparing the AO-SLO image with the wide-field images for that eye.

To evaluate cones, we applied the automated cone labeling process of Li and Roorda, which uses an algorithm implemented in MATLAB (Mathworks Inc., Natick, MA, USA) and a function from the MATLAB Image Processing Toolbox



4
5
6
7
8
9
10
11
12
13
14
15
16
17
18
19
20
21
22
23
24
25
26
27
28
29
30
31
32
33
34
35
36
37
38
39
40
41
42
43
44
45
46
47
48
49
50
51
52
53
54
55
56
57
58
59
60
61
62
63
64
65

(IPT).⁴⁸ After automated cone labeling, 2 independent experienced observers examined each image; if cones were visible but had not been labeled, the observer manually labeled the areas where cones were visible and entered this area into the computer software program.

As has been reported for similar systems,²⁸⁻⁴⁴ we found that our system did not always allow clear visualization of individual cones within much of the central fovea. However, we could clearly distinguish individual cones > .2 mm from the center of the fovea. Therefore, we obtained an estimate of cone density in areas .5 mm from the foveal center by instructing the computer software program to divide the number of cones in each imaging area by the size of the area. We measured cone density in each of 4 directions (superior, lower, nasal, and temporal), and the mean density was calculated from the densities in all 4 directions. To obtain accurate lengths of scans, we corrected the magnification effect in each eye by using the adjusted axial length method reported by Bennett et al.⁴⁹

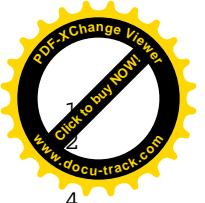
We quantified the extent of the dark areas (areas lacking cones) in AO-SLO images by having the aforementioned independent experienced observers define and measure the dark areas in each eye using the Java-based image-processing software program ImageJ (National Institutes of Health [NIH], Bethesda, MD, USA). The total dark area in each eye was calculated as the mean of the total dark areas measured by the 2 observers.

Spectral-domain Optical Coherence Tomography Evaluation of Photoreceptor Layer Features and Retinal Thickness Measurements

We used the Spectralis HRA+OCT (Heidelberg Engineering, Dossenheim, Germany) to perform SD-OCT before and after surgery in all patient eyes. We obtained and evaluated 12 serial radial B-scan images through the fovea of each eye.

Photoreceptor Inner and Outer Segment Junction Disruptions

We identified 2 abnormalities in the IS/OS on preoperative SD OCT images (Fig 1): (1) diffuse decreased reflectivity that extended to the outside of the MH (designated as “preoperative IS/OS decreased reflectivity”); and (2) a focal disruption or defect in the line of reflectivity representing the OS, along with the



4
5
6
7
8
9
10
11
12
13
14
15
16
17
18
19
20
21
22
23
24
25
26
27
28
29
30
31
32
33
34
35
36
37
38
39
40
41
42
43
44
45
46
47
48
49
50
51
52
53
54
55
56
57
58
59
60
61
62
63
64
65

ELM, curling toward the top of the image (externally), along the sides of the defect in the fovea (designated as “preoperative OS defect in the fluid cuff”).

On postoperative SD-OCT images, we defined abnormalities such as postoperative IS/OS disruption in a healed MH as decreased reflectivity of the IS/OS in the fovea (Fig 2). We also identified moderately reflective foveal lesions (Fig 2).

We measured IS/OS reflectivity using the “plot profile” analysis function of ImageJ. This function displays a 2-dimensional graph of the intensities of pixels along a line within the image, with the X-axis representing distance along the line and the Y-axis representing pixel intensity. The border of the IS/OS decreased reflectivity was defined as the line on the gray-scale image along which IS/OS reflectivity had diminished by 2 standard deviations (SD) from IS/OS reflectivity in the unaffected peripheral macula. We calculated the mean diameter of the decreased reflectivity areas from 12 radial B-scan images.

Preoperative OS defects in the fluid cuff and postoperative moderately reflective foveal lesions were evaluated independently by 2 graders in the Kyoto University OCT Reading Center, both experienced in evaluating OCT images and unaware of any clinical information, including AO-SLO findings. When their evaluations did not agree, a third grader (SO) was consulted and the results were discussed until consensus was reached.

Other Measurements

We manually measured additional anatomic parameters (see below) on SD-OCT images, both before and after surgery to close MH. For all measurements, reports and analyses were based on 12 radial B-scan images through the center of the fovea.

On preoperative images, we measured the basal diameter of the MH (averaged across all 12 B-scan images), MH height (maximal height of elevated foveal retina), and minimum diameter of the MH (minimum distance between the separated outer segments) by using the digital caliper tool built into the SD-OCT system (Fig 3).

On postoperative images (obtained concurrently with AO-SLO), we measured the thickness of the outer nuclear layer (ONL; the distance between the vitreoretinal interface and ELM) and the thickness of inner and outer segments (the



4
5
6
7
8
9
10
11
12
13
14
15
16
17
18
19
20
21
22
23
24
25
26
27
28
29
30
31
32
33
34
35
36
37
38
39
40
41
42
43
44
45
46
47
48
49
50
51
52
53
54
55
56
57
58
59
60
61
62
63
64
65

distance between the ELM and the inner border of the RPE), at the center of the fovea (Fig 3).

Microperimetry: Retinal Sensitivity Measurements

We used fundus-monitoring microperimetry (MP) to measure retinal sensitivity. The MP-1 (NIDEK) software can be set to automatically track fundus movements and evaluate every acquired frame for shifts in the directions of the X- and Y-axes of the fundus with respect to a reference image obtained by an infrared camera at the beginning of the examination.

We used a 4-2-staircase strategy with a Goldmann size III stimulus against a white background with illumination of 1.27 cd/m² to examine 33 stimulus locations covering the central 6 degrees. The differential luminance, defined as the difference between stimulus and background luminances, was 127 cd/m² at 0 decibels (dB) of stimulation. Maximum stimulus attenuation was 20 dB, and the duration of the stimulus was 200 ms.

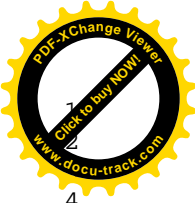
In the current study, mean foveal sensitivity was defined as the mean of retinal sensitivities measured at 9 different points in the fovea.

Macular Hole Repair

MH was repaired in each case by standard 3-port pars plana vitrectomy (23-gauge system). Before vitrectomy, all phakic eyes underwent phacoemulsification and implantation of a posterior chamber intraocular lens. After core vitrectomy with intravitreal injection of triamcinolone acetonide to visualize the vitreous gel, we detached the posterior vitreous if detachment had not yet occurred, peeled the internal limiting membrane (ILM) using 0.05% indocyanine green (ICG) dye or triamcinolone acetonide, and performed fluid-gas exchange followed by flushing with a mixed non-expansile solution of 25% sulfur hexafluoride. Postoperatively, patients were instructed to remain facedown for 7 days.

Surgical MH repair was considered anatomically successful when postoperative biomicroscopy and SD-OCT revealed a closed MH.

Statistical Analysis



4
5
6
7
8
9
10
11
12
13
14
15
16
17
18
19
20
21
22
23
24
25
26
27
28
29
30
31
32
33
34
35
36
37
38
39
40
41
42
43
44
45
46
47
48
49
50
51
52
53
54
55
56
57
58
59
60
61
62
63
64
65

We used paired *t*-tests to compare pre- and post-surgery measurements of mean BCVA, foveal sensitivity, and IS/OS abnormality. Student *t*-tests were used to evaluate cone density and the area of cone loss (dark area). We calculated the Pearson product moment correlation coefficient to determine associations between cone density/dark (cone loss) area and other variables.

All statistical evaluations were performed using the commercially available software program SPSS v.17 (SPSS Inc., Chicago, IL, USA). Significance was defined as $P < .05$.

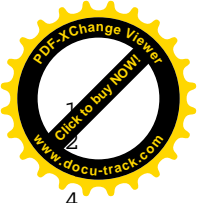
RESULTS

All patients underwent anatomically successful MH closure with no complications. Table 1 summarizes characteristics of patients and eyes prior to, and at, surgery. The median time from onset of visual symptoms to MH surgery was 2 months, and mean preoperative logMAR was .584. Almost half of eyes had stage 2 MH; the mean minimum diameter of the MH was 303.5 μm . Before surgery, the mean IS/OS decreased reflectivity size was 1447.8 μm .

Table 2 summarizes characteristics of eyes at 6 months after surgical repair of MH. Surgical treatment of MH significantly improved mean visual acuity (logMAR values) and reduced mean diameter of IS/OS decreased reflectivity (both $P < .001$). The ONL and the inner and outer segments at the foveal center were thinner in surgically treated eyes than in normal eyes ($P = .038$ and $P = .002$, respectively). The postoperative diameter of the IS/OS decreased reflectivity was smaller than the preoperative basal diameter of the MH in all eyes.

After MH repair, AO-SLO revealed the presence of dark areas totaling .004 to .754 mm^2 in the foveae of all treated eyes (Figs 4-7). This was true even in eyes for which the postoperative SD-OCT did not reveal any visible defects in the IS/OS (Fig 4). Mean cone density in eyes with surgically closed MH was 19,650 cones/ mm^2 , which was significantly lower than in normal eyes ($P = .003$; Table 2).

Preoperative logMAR visual acuity was correlated with postoperative cone density ($P = .024$, $R = -.490$; Table 3). Postoperatively, lower cone density correlated with poorer logMAR visual acuity ($P < .001$, $R = -.742$), lower mean foveal sensitivity ($P < .001$, $R = .812$), and thinner inner and outer segments at the foveal center ($P = .014$, $R = .530$; Table 3). Cone density was significantly lower



4
5
6
7
8
9
10
11
12
13
14
15
16
17
18
19
20
21
22
23
24
25
26
27
28
29
30
31
32
33
34
35
36
37
38
39
40
41
42
43
44
45
46
47
48
49
50
51
52
53
54
55
56
57
58
59
60
61
62
63
64
65

after surgery in eyes that had pre-surgery OS defects in the fluid cuff ($P = .018$) and moderately reflective foveal lesions after surgery ($P < .001$) (Figs 4-7, Table 4).

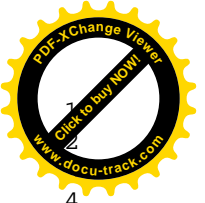
The size of dark areas was positively correlated with symptom duration before surgery ($P < .001$, $R = .731$) and, postoperatively, with poorer logMAR visual acuity ($P = .003$, $R = .613$), lower mean foveal sensitivity ($P = .006$, $R = -.651$), thinner inner and outer segments at the center of the fovea ($P = .044$, $R = -.444$), and larger IS/OS decreased reflectivity size ($P = .013$, $R = .531$) (Table 3). On AO-SLO images, dark areas were significantly larger in eyes that had OS defects in the fluid cuff before surgery ($P = .001$) (Figs 4-7; Table 4), and moderately reflective foveal lesions after surgery ($P = .001$) (Figs 6, 7, Table 4).

Cone density was negatively correlated with the size of dark areas within the cone mosaic on AO-SLO ($P = .001$, $R = -.667$).

DISCUSSION

To date, many studies using conventional TD-OCT^{9,10,12,13 18,19} or SD-OCT²¹⁻²⁴ have reported a possible association between the integrity of the photoreceptor layer and visual improvement after successful MH repair. Several investigators have reported that a disrupted photoreceptor IS/OS line^{9,10,12,13 18,19, 21-23} and/or disrupted ELM²⁴ may be closely associated with postoperative visual impairment. However, these studies could not ascertain how the individual photoreceptors are damaged after successful MH repair, or how these damages are correlated with decreased visual function. Our results provide evidence that structural damage to larger areas of photoreceptor damages correlated with greater decreases in visual function in eyes with surgically closed MH. Examples of this damage are the dark regions in the cone mosaics of eyes with closed MH (Figs 5 and 7). We propose that these represent abnormalities at the photoreceptor level—possibly loss of the cone photoreceptor cells.

This proposal is based on several findings. First, these dark areas were only present within the fovea and/or parafovea of eyes with surgically closed MH, and were absent from normal eyes. Second, a comparison of AO-SLO images with wide-field SLO images or fundus photographs allowed us to rule out the possibility that the dark areas represented shadows of blood vessels. Moderately reflective foveal lesions seem to have little effect on the penetration of light reflected from the



4
5
6
7
8
9
10
11
12
13
14
15
16
17
18
19
20
21
22
23
24
25
26
27
28
29
30
31
32
33
34
35
36
37
38
39
40
41
42
43
44
45
46
47
48
49
50
51
52
53
54
55
56
57
58
59
60
61
62
63
64
65

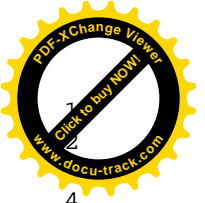
deeper layers. In fact, on SD-OCT, which uses a light source with a wavelength (840 nm) identical to that of our AO-SLO system, there were no shadows in the photoreceptor layer or RPE. Third, the dark areas on the AO-SLO images positively correlated with the areas of disruption in the IS/OS on SD-OCT images. These results are consistent with those of previous studies of eyes with other retinal diseases,^{38, 42, 44} in which the dark areas seen in the AO images corresponded with the areas of disruption in the IS/OS, or the cone outer segment tip in corresponding SD-OCT images.

It is notable that we saw dark areas in all eyes after MH repair—even in those in which SD-OCT demonstrated an apparently intact IS/OS. We believe that in cases where the IS/OS appeared intact on SD-OCT, there were actually micro-abnormalities in the IS/OS that we could not see on SD-OCT because of its lower resolution. Commercially available SD-OCT systems (without AO) have a lateral resolution of approximately 20 μm , while the AO-SLO, which has a lateral resolution of 3 μm , detected abnormalities that were ~5-20 μm wide.

In the current study, decreased cone density and larger total dark area in the fovea on AO-SLO correlated with worse visual acuity and worse retinal sensitivity in the fovea (Table 3). This pattern is similar to previously reported correlations between the sizes of defects in the IS/OS and/or ELM and the severity of postoperative visual impairment; these results were obtained using SD-OCT techniques²¹⁻²⁴. Cumulatively, all of these findings suggest that functional impairment may be closely associated with foveal photoreceptor alterations in eyes with closed MH.

Another significant finding of our study was that lower cone density and larger dark areas in the fovea on AO-SLO correlated with thinner inner and outer segments on SD-OCT (Table 3) 6 months after surgical closure of MH. This pattern suggests that decreased inner and outer segment thickness may reflect more severe structural disturbance of the photoreceptor layer.

We found that postoperative cone density was significantly lower, and dark area was significantly larger, when an OS defect in the fluid cuff was present preoperatively (Table 4). This led us to hypothesize that, when an MH forms, cone photoreceptors are pulled out of the RPE as a result of anteroposterior traction on the photoreceptor layer (and, therefore, cone photoreceptors) caused by detachment of the perifoveal posterior vitreous. This is supported not only by our

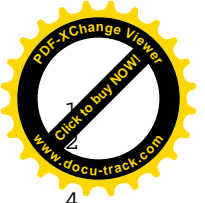


4
5
6
7
8
9
10
11
12
13
14
15
16
17
18
19
20
21
22
23
24
25
26
27
28
29
30
31
32
33
34
35
36
37
38
39
40
41
42
43
44
45
46
47
48
49
50
51
52
53
54
55
56
57
58
59
60
61
62
63
64
65

own observations, but also by previous research results. For instance, an immunohistochemical analysis of the operculas of stage 3 full-thickness MH specimens obtained during vitrectomies revealed that 67% of the opercula contained neuroretinal tissue, including cone photoreceptors⁵⁰; this suggests that the MHs arose from avulsion of foveal neural tissue. Further, histopathologic studies of eyes with MH showed disruption of the photoreceptor layer surrounding the MH.⁵¹ Thus, observation of an OS defect in the fluid cuff on SD-OCT may indicate the loss or atrophy of photoreceptors. If these patterns do indeed indicate dissociation of the cone photoreceptors from the RPE, an OS defect in the fluid cuff is a reflection of severe damage to cones, and would be expected to be closely associated with postoperative cone abnormalities—as was the case in our study. Longer duration of symptoms of MH would be expected to cause more extensive damage to cone photoreceptors in the fluid cuff, and indeed our study showed a correlation between larger dark area (area of cone loss) and longer duration of symptoms before surgery for MH.

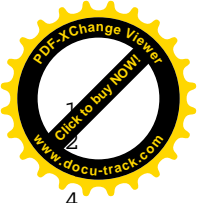
Histopathologic studies of repaired MHs have shown that photoreceptor cells atrophy and are replaced by Müller cells and/or astrocytes at the site of MH.⁵²⁻⁵⁴ These cellular changes may underlie the moderately reflective lesions we saw in the fovea of treated eyes. Such moderately reflective foveal lesions, which were first reported by Ko et al. on ultrahigh-resolution OCT images, are considered to represent glial cell proliferation at the foveal defect during MH closure.¹⁹ Oh et al. also reported seeing moderately reflective foveal lesions, which they described as being of a “glial sealing type;” these were found to be correlated with poorer postoperative BCVA and larger postoperative size of the IS/OS defect.²³ In the current study, the eyes that had moderately reflective foveal lesions had lower cone density and larger dark areas on AO-SLO (Table 4). Based on these findings, we hypothesize that the pattern of foveal reconstruction in closed MH may depend on a balance between the proliferation of the glial cells filling the foveal defect and the bridging of the photoreceptor cell bodies with subsequent elongation of the photoreceptor outer segments.

Our study has several limitations: (1) Although it has better lateral resolution than commercially available SD-OCT, our AO imaging equipment was still unable to clearly show individual cone photoreceptors in the foveal center.²⁰⁻⁴⁴ However, each dark area representing cone loss was larger than the diameter of



4
5
6
7
8
9
10
11
12
13
14
15
16
17
18
19
20
21
22
23
24
25
26
27
28
29
30
31
32
33
34
35
36
37
38
39
40
41
42
43
44
45
46
47
48
49
50
51
52
53
54
55
56
57
58
59
60
61
62
63
64
65

cones in the central fovea. In fact, dark area could be detectable near the center of the fovea even though the individual cones were not resolved in the same location. (2) We could not evaluate AO-SLO images preoperatively and we were forced to exclude an eye that developed foveal detachment postoperatively, because we were unable to adequately focus on photoreceptors using the AO-SLO system in these status. Nevertheless, in the great majority of eyes in which MH was surgically closed (21 of 22 eyes), our AO-SLO system allowed us to detect and measure damage to individual photoreceptor cells. Cone loss was seen in all eyes with surgically closed MH. Preoperative defects in the outer segments in the fluid cuff were associated with poor postoperative photoreceptor status. Longer symptom duration may result in a larger area of photoreceptor loss after surgery. Postoperative photoreceptor status, which was closely associated with visual acuity and retinal sensitivity, may be predicted from these preoperative clinical characteristics. Our study shows that AO-SLO imaging is a useful and quantitative tool for detecting photoreceptor abnormalities and their association with visual acuity and retinal sensitivity in eyes with closed MH. We are therefore planning prospective longitudinal studies using AO-SLO to learn more about the relationship of dark areas/decreased cone density in the healing process of MH, with the hope that this knowledge will point the way to better management of this disease.



4
5
6
7
8
9
10
11
12
13
14
15
16
17
18
19
20
21
22
23
24
25
26
27
28
29
30
31
32
33
34
35
36
37
38
39
40
41
42
43
44
45
46
47
48
49
50
51
52
53
54
55
56
57
58
59
60
61
62
63
64
65

ACKNOWLEDGMENTS

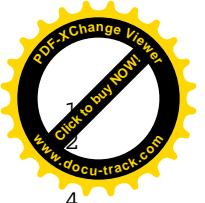
Funding/Support: This research was supported in part by the New Energy and Industrial Technology Development Organization (NEDO; P05002), Kawasaki, Japan.

Financial disclosures: Masanori Hangai and Nagahisa Yoshimura are paid members of the advisory boards of NIDEK. Masaaki Hanebuchi is an employee of NIDEK. Sotaro Ooto, Kohei Takayama, and Naoko Ueda-Arakawa have no financial interests to disclose.

Author contribution: Conception and design (S.O.) Analysis and interpretation (S.O., M.Hangai) Writing the article (S.O., M.Hangai) Critical revision of the article (S.O., M.Hangai, N.Y.) Final approval of the article (S.O., M.Hangai, K.T., N.U.A., M.Hanebuchi, N.Y.) Data collection (K.T., N.U.A.) Provision of materials (M.Hanebuchi) Statistical expertise (S.O., M.Hangai) Obtaining funding (M.Hangai, M.Hanebuchi, N.Y.) Literature search (S.O., M.Hangai) Technical support (M.Hanebuchi)

Statement of conformity with author information: All the investigations in this study adhered to the tenets of the Declaration of Helsinki, and this prospective study was approved by the Institutional Review Board and the Ethics Committee of Kyoto University Graduate School of Medicine. The nature of the study, participation in its research, and its possible consequences were explained to the study candidates, after which written informed consent was obtained from all participants.

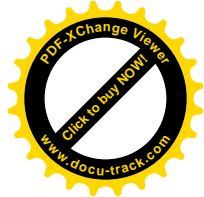
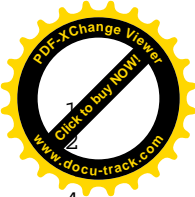
Other Acknowledgements: We wish to thank the imaging specialists of Kyoto University OCT Reading Center (Mayumi Yoshida and Akiko Hirata) for evaluating AO-SLO and SD-OCT images.



4
5
6
7
8
9
10
11
12
13
14
15
16
17
18
19
20
21
22
23
24
25
26
27
28
29
30
31
32
33
34
35
36
37
38
39
40
41
42
43
44
45
46
47
48
49
50
51
52
53
54
55
56
57
58
59
60
61
62
63
64
65

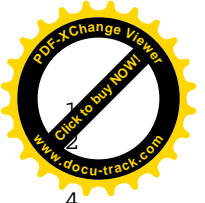
REFERENCES

1. Kelly NE, Wendel RT. Vitreous surgery for idiopathic macular holes. Results of a pilot study. *Arch Ophthalmol* 1991;109(5):654-659.
2. Smiddy WE, Feuer W, Cordahi G. Internal limiting membrane peeling in macular hole surgery. *Ophthalmology* 2001;108(8):1471-1476.
3. Brooks HL Jr. Macular hole surgery with and without internal limiting membrane peeling. *Ophthalmology* 2000;107(10):1939-1948.
4. Tranos PG, Ghazi-Nouri SM, Rubin GS, Adams ZC, Charteris DG. Visual function and subjective perception of visual ability after macular hole surgery. *Am J Ophthalmol* 2004;138(6):995-1002.
5. Haritoglou C, Reiniger IW, Schaumberger M, Gass CA, Priglinger SG, Kampik A. Five-year follow-up of macular hole surgery with peeling of the internal limiting membrane: update of a prospective study. *Retina* 2006;26(6):618-622.
6. Meng Q, Zhang S, Ling Y, Cui D, Jin Y. Long-term anatomic and visual outcomes of initially closed macular holes. *Am J Ophthalmol* 2011;151(5):896-900.e2.
7. Hee MR, Puliafito CA, Wong C, et al. Optical coherence tomography of macular holes. *Ophthalmology* 1995;102(5):748-756.
8. Ip MS, Baker BJ, Duker JS, et al. Anatomical outcomes of surgery for idiopathic macular hole as determined by optical coherence tomography. *Arch Ophthalmol* 2002;120(1):29-35.
9. Kitaya N, Hikichi T, Kagokawa H, Takamiya A, Takahashi A, Yoshida A. Irregularity of photoreceptor layer after successful macular hole surgery prevents visual acuity improvement. *Am J Ophthalmol* 2004;138(2):308-310.
10. Villate N, Lee JE, Venkatraman A, Smiddy WE. Photoreceptor layer features in eyes with closed macular holes: optical coherence tomography findings and correlation with visual outcomes. *Am J Ophthalmol* 2005;139(2):280-289.
11. Kusahara S, Teraoka Escano MF, Fujii S, et al. Prediction of postoperative visual outcome based on hole configuration by optical coherence tomography in eyes with idiopathic macular holes. *Am J Ophthalmol* 2004;138(5):709-716.
12. Moshfeghi AA, Flynn HW Jr, Elnor SG, Puliafito CA, Gass JD. Persistent outer retinal defect after successful macular hole repair. *Am J Ophthalmol* 2005;139(1):183-184.



4
5
6
7
8
9
10
11
12
13
14
15
16
17
18
19
20
21
22
23
24
25
26
27
28
29
30
31
32
33
34
35
36
37
38
39
40
41
42
43
44
45
46
47
48
49
50
51
52
53
54
55
56
57
58
59
60
61
62
63
64
65

13. Baba T, Yamamoto S, Arai M, et al. Correlation of visual recovery and presence of photoreceptor inner/outer segment junction in optical coherence images after successful macular hole repair. *Retina* 2008;28(3):453-458.
14. Ruiz-Moreno JM, Staicu C, Pinero DP, Montero J, Lugo F, Amat P. Optical coherence tomography predictive factors for macular hole surgery outcome. *Br J Ophthalmol* 2008;92(5):640-644.
15. Kang SW, Lim JW, Chung SE, Yi CH. Outer foveolar defect after surgery for idiopathic macular hole. *Am J Ophthalmol* 2010;150(4):551-557.
16. Kawano H, Uemura A, Sakamoto T. Incidence of outer foveal defect after macular hole surgery. *Am J Ophthalmol* 2011;151(2):318-322.
17. Christensen UC, Kroyer K, Sander B, Larsen M, la Cour M. Prognostic significance of delayed structural recovery after macular hole surgery. *Ophthalmology* 2009;116(12):2430-2436.
18. Drexler W, Sattmann H, Hermann B, et al. Enhanced visualization of macular pathology with the use of ultrahigh-resolution optical coherence tomography. *Arch Ophthalmol* 2003;121(5):695-706.
19. Ko TH, Fujimoto JG, Schuman JS, et al. Comparison of ultrahigh- and standard-resolution optical coherence tomography for imaging macular pathology. *Ophthalmology* 2005;112(11):1922.e1-15.
20. Hangai M, Ojima Y, Gotoh N, et al. Three-dimensional imaging of macular holes with high-speed optical coherence tomography. *Ophthalmology* 2007;114(4):763-773.
21. Chang LK, Koizumi H, Spaide RF. Disruption of the photoreceptor inner segment-outer segment junction in eyes with macular holes. *Retina* 2008;28(7):969-975.
22. Sano M, Shimoda Y, Hashimoto H, Kishi S. Restored photoreceptor outer segment and visual recovery after macular hole closure. *Am J Ophthalmol* 2009;147(2):313-318.e1.
23. Oh J, Smiddy WE, Flynn HW Jr, Gregori G, Lujan B. Photoreceptor inner/outer segment defect imaging by spectral domain OCT and visual prognosis after macular hole surgery. *Invest Ophthalmol Vis Sci* 2010;51(3):1651-1658.
24. Wakabayashi T, Fujiwara M, Sakaguchi H, Kusaka S, Oshima Y. Foveal microstructure and visual acuity in surgically closed macular holes: spectral-



4
5
6
7
8
9
10
11
12
13
14
15
16
17
18
19
20
21
22
23
24
25
26
27
28
29
30
31
32
33
34
35
36
37
38
39
40
41
42
43
44
45
46
47
48
49
50
51
52
53
54
55
56
57
58
59
60
61
62
63
64
65

domain optical coherence tomographic analysis. *Ophthalmology* 2010;117(9):1815-1824.

25. Bottoni F, De Angelis S, Luccarelli S, Cigada M, Staurenghi G. The dynamic healing process of idiopathic macular holes after surgical repair: a spectral-domain optical coherence tomography study. *Invest Ophthalmol Vis Sci* 2011;52(7):4439-4446.

26. Chung H, Shin CJ, Kim JG, Yoon YH, Kim HC. Correlation of microperimetry with fundus autofluorescence and spectral-domain optical coherence tomography in repaired macular holes. *Am J Ophthalmol* 2011;151(1):128-136.e3.

27. Takahashi A, Nagaoka T, Ishiko S, Kameyama D, Yoshida A. Foveal anatomic changes in a progressing stage 1 macular hole documented by spectral-domain optical coherence tomography. *Ophthalmology* 2010;117(4):806-810.

28. Liang J, Williams DR, Miller DT. Supernormal vision and high-resolution retinal imaging through adaptive optics. *J Opt Soc Am A Opt Image Sci Vis* 1997;14(11):2884-2892.

29. Roorda A, Williams DR. The arrangement of the three cone classes in the living human eye. *Nature* 1999;397(6719):520-522.

30. Roorda A, Williams DR. Optical fiber properties of individual human cones. *J Vis* 2002;2(5):404-412.

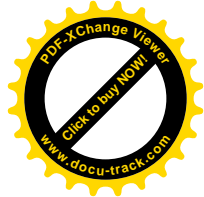
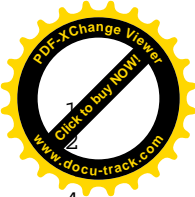
31. Roorda A, Romero-Borja F, Donnelly WJ III, et al. Adaptive optics scanning laser ophthalmoscopy. *Opt Express* 2002;10(9):405-412.

32. Pallikaris A, Williams DR, Hofer H. The reflectance of single cones in the living human eye. *Invest Ophthalmol Vis Sci* 2003;44(10):4580-4592.

33. Carroll J, Neitz M, Hofer H, et al. Functional photoreceptor loss related with adaptive optics: an alternate cause of color blindness. *Proc Natl Acad Sci USA* 2004;101(22):8461-8466.

34. Wolfing JI, Chung M, Carroll J, et al. High-resolution retinal imaging of cone-rod dystrophy. *Ophthalmology* 2006;113(6):1019.e1.

35. Choi SS, Doble N, Hardy JL, et al. In vivo imaging of the photoreceptor mosaic in retinal dystrophies and correlations with visual function. *Invest Ophthalmol Vis Sci* 2006;47(5):2080-2092.



4
5
6
7
8
9
10
11
12
13
14
15
16
17
18
19
20
21
22
23
24
25
26
27
28
29
30
31
32
33
34
35
36
37
38
39
40
41
42
43
44
45
46
47
48
49
50
51
52
53
54
55
56
57
58
59
60
61
62
63
64
65

36. Duncan JL, Zhang Y, Gandhi J, et al. High-resolution imaging with adaptive optics in patients with inherited retinal degeneration. *Invest Ophthalmol Vis Sci* 2007;48(7):3283-3291.

37. Yoon MK, Roorda A, Zhang Y, et al. Adaptive optics scanning laser ophthalmoscopy images in a family with the mitochondrial DNA T8993C mutation. *Invest Ophthalmol Vis Sci* 2009;50(4):1838-1847.

38. Kitaguchi Y, Fujikado T, Bessho K, et al. Adaptive optics fundus camera to examine localized changes in the photoreceptor layer of the fovea. *Ophthalmology* 2008;115(10):1771-1777.

39. Choi SS, Zawadzki RJ, Keltner JL, Werner JS. Changes in cellular structures revealed by ultra-high resolution retinal imaging in optic neuropathies. *Invest Ophthalmol Vis Sci* 2008;49(5):2103-2119.

40. Marmor MF, Choi SS, Zawadzki RJ, Werner JS. Visual insignificance of the foveal pit: reassessment of foveal hypoplasia as fovea plana. *Arch Ophthalmol* 2008;126(7):907-913.

41. Choi SS, Zawadzki RJ, Greiner MA, et al. Fourier-domain optical coherence tomography and adaptive optics retinal nerve fiber layer loss and photoreceptor changes in a patient with optic nerve drusen. *J Neuro-Ophthalmol* 2008;28(2):120-125.

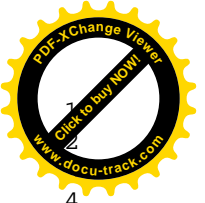
42. Ooto S, Hangai M, Sakamoto A, et al. High-resolution imaging of resolved central serous chorioretinopathy using adaptive optics scanning laser ophthalmoscopy. *Ophthalmology* 2010;117(9):1800-1809.

43. Ooto S, Hangai M, Takayama K, et al. High-resolution imaging of the photoreceptor layer in epiretinal membrane using adaptive optics scanning laser ophthalmoscopy. *Ophthalmology* 2011;118(5):873-881.

44. Ooto S, Hangai M, Takayama K, et al. High-resolution photoreceptor imaging in idiopathic macular telangiectasia type 2 using adaptive optics scanning laser ophthalmoscopy. *Invest Ophthalmol Vis Sci* 52(8):5541-5550.

45. Gass JD. Reappraisal of biomicroscopic classification of stages of development of a macular hole. *Am J Ophthalmol* 1995;119(6):752-759.

46. Burns SA, Tumbar R, Elsner AE, Ferguson D, Hammer DX. Large-field-of view, modular, stabilized, adaptive-optics-based scanning laser ophthalmoscope. *J Opt Soc Am A Opt Image Sci Vis* 2007;24(5):1313-1326.



4
5
6
7
8
9
10
11
12
13
14
15
16
17
18
19
20
21
22
23
24
25
26
27
28
29
30
31
32
33
34
35
36
37
38
39
40
41
42
43
44
45
46
47
48
49
50
51
52
53
54
55
56
57
58
59
60
61
62
63
64
65

47. Ferguson RD, Zhong Z, Hammer DX, et al. Adaptive optics scanning laser ophthalmoscope with integrated wide-field retinal imaging and tracking. *J Opt Soc Am A Opt Image Sci Vis* 2010;27(11):A265-277.

48. Li KY, Roorda A. Automated identification of cone photoreceptors in adaptive optics retinal images. *J Opt Soc Am A Opt Image Sci Vis* 2007;24(5):1358-1363.

49. Bennett AG, Rudnicka AR, Edgar DF. Improvements on Littmann's method of determining the size of retinal features by fundus photography. *Graefes Arch Clin Exp Ophthalmol* 1994;232(6):361-367.

50. Ezra E, Fariss RN, Possin DE, et al. Immunocytochemical characterization of macular hole opercula. *Arch Ophthalmol* 2001;119(2):223-231.

51. Frangieh GT, Green WR, Engel HM. A histopathologic study of macular cysts and holes. *Retina* 1981;1(4):311-336.

52. Funata M, Wendel RT, de la Cruz Z, Green WR. Clinicopathologic study of bilateral macular holes treated with pars plana vitrectomy and gas tamponade. *Retina* 1992;12(4):289-298.

53. Madreperla SA, Geiger GL, Funata M, de la Cruz Z, Green WR. Clinicopathologic correlation of a macular hole treated by cortical vitreous peeling and gas tamponade. *Ophthalmology* 1994;101(4):682-686.

54. Rosa RH Jr, Glaser BM, de la Cruz Z, Green WR. Clinicopathologic correlation of an untreated macular hole and a macular hole treated by vitrectomy, transforming growth factor-beta 2, and gas tamponade. *Am J Ophthalmol* 1996;122(6):853-863.

4
5
6
7
8
9
10
11
12
13
14
15
16
17
18
19
20
21
22
23
24
25
26
27
28
29
30
31
32
33
34
35
36
37
38
39
40
41
42
43
44
45
46
47
48
49
50
51
52
53
54
55
56
57
58
59
60
61
62
63
64
65

Figure Captions

Figure 1. Spectral-domain optical coherence tomography (SD-OCT) images of eyes with idiopathic macular holes. (Top) In this eye, the reflectivity of the photoreceptor inner segment/outer segment junction (IS/OS) is 2 standard deviations lower in the area that extends to the outside of the macular hole (between arrowheads; designated as “IS/OS decreased reflectivity”) than in the unaffected peripheral macula. However, this IS/OS line appears continuous in the fluid cuff (arrows), where it can be seen adjacent to the external limiting membrane (ELM). (Bottom) In this eye, the reflectivity of the IS/OS has decreased in the area that extends to the outside of the macular hole (between arrowheads; designated as “IS/OS decreased reflectivity”) and shows defects (arrows; defined as “outer segment [OS] defect in the fluid cuff”) where it lies against the ELM in the fluid cuff.

Figure 2. Spectral-domain optical coherence tomography (SD-OCT) images of eyes with surgically closed macular holes. (Top) The outer nuclear layer (ONL) and the photoreceptor inner segment/outer segment junction (IS/OS) are intact. (Bottom) A moderately reflective lesion (arrow) is seen in the fovea and the IS/OS is disrupted (between arrowheads; designated as “IS/OS decreased reflectivity”).

Figure 3. Spectral-domain optical coherence tomography (SD-OCT) images of eyes with macular holes (MH), showing anatomic parameters measured before (Top) and after (Bottom) surgery performed to close the hole. (Top) Preoperative measurements included: m , the minimum diameter of the MH; b , basal diameter of the MH; and h , height of the MH. IS/OS = photoreceptor inner and outer segment junction, RPE = retinal pigment epithelium. (Bottom) Postoperative measurements included the thickness of the outer nuclear layer (ONL), which was measured between the vitreoretinal interface and external limiting membrane (ELM), and the thickness of inner and outer segments, measured between the ELM and RPE.

Figure 4. Images of the right eye of a 65-year-old woman with idiopathic macular hole (MH) (stage 4) with a Snellen equivalent best-corrected visual acuity (BCVA) of 20/60 before, and 20/15 after, surgery to close the MH. Top: Preoperative spectral-domain optical coherence tomography (SD-OCT) image showing a full-thickness MH. The reflectivity of the junction of the photoreceptor inner and outer

4
5
6
7
8
9
10
11
12
13
14
15
16
17
18
19
20
21
22
23
24
25
26
27
28
29
30
31
32
33
34
35
36
37
38
39
40
41
42
43
44
45
46
47
48
49
50
51
52
53
54
55
56
57
58
59
60
61
62
63
64
65

segment layers (IS/OS) has decreased in the area between the blue arrowheads but is continuous (blue arrows) in the fluid cuff, where it lies adjacent to the external limiting membrane (ELM). m = MH minimum diameter (288 μm); b = MH basal diameter (720 μm); h = MH height (404 μm). (2nd row, 3rd row, bottom) Images 6 months after surgery (BCVA 20/15). (2nd row, left) Fundus photograph showing closed MH. (2nd row, middle) Infrared image with green arrows indicating the directions of scans shown in 3rd row and bottom and a white box indicating the sizes of the double-headed arrows in 3rd row and bottom. (2nd row, right) Microperimetry results show normal foveal sensitivity (mean foveal sensitivity = 18.0 dB). (3rd row-bottom) SD-OCT images. ELM = external limiting membrane. (3rd row) Horizontal scan through the center of the fovea, in the direction of the horizontal arrow in 2nd row (middle), showing that the IS/OS is intact. The inner surface of the temporal side of the fovea is irregular, but the outer nuclear layer (ONL) is intact. (Bottom) Vertical line scan through the center of the fovea, in the direction of the vertical arrow in 2nd row (middle), showing intact IS/OS and ONL. RPE = retinal pigment epithelium.

Figure 5. Adaptive optics scanning laser ophthalmoscopy (AO-SLO) images of an eye with a surgically closed macular hole (the same eye shown in Fig 4). Small areas of darkness (arrows) are seen on AO-SLO images of the area indicated by the white box in the middle of the 2nd row of Fig 4. The total area of these dark areas was .012 mm², and the mean cone density .5 mm from the center of the fovea was 27,343 cones/mm². The asterisk indicates the center of the fovea. The bottom 3 images are high-magnification views of the areas outlined by the white boxes. Scale bar = 100 μm .

Figure 6. Images of the left eye of a 61-year-old woman with idiopathic macular hole (MH) (stage 2) with a Snellen equivalent best-corrected visual acuity (BCVA) of 20/60 before, and 20/50 after, surgery. (Top) The spectral-domain optical coherence tomography (SD-OCT) image shows a full-thickness macular hole. The reflectivity of the junction of the photoreceptor inner and outer segment layers (IS/OS) has decreased between the blue arrowheads and defects of the outer segment are seen in the fluid cuff (red arrow). m = MH minimum diameter (252

4
5
6
7
8
9
10
11
12
13
14
15
16
17
18
19
20
21
22
23
24
25
26
27
28
29
30
31
32
33
34
35
36
37
38
39
40
41
42
43
44
45
46
47
48
49
50
51
52
53
54
55
56
57
58
59
60
61
62
63
64
65

μm); b = MH basal diameter (942 μm); h = MH height (465 μm); ELM = external limiting membrane. (2nd row, 3rd row, bottom) Images 6 months after surgery (BCVA 20/50). (2nd row, left) Fundus photograph showing closed MH. (2nd row, middle) Infrared image with green arrows indicating the directions of the scans producing the images in 3rd row and bottom, and a white box indicating the size of the double-headed arrows in 3rd row and bottom. (2nd row, right) Microperimetry showing relative central scotoma (mean foveal sensitivity = 13.2 dB). (3rd row-bottom) SD-OCT images. (3rd row) Horizontal scan through the center of the fovea in the direction of the horizontal arrow in 2nd row (middle) showing decreased reflectivity (between red arrowheads) of the IS/OS in the fovea; in this eye, the IS/OS decreased reflectivity (428 μm) was smaller than the preoperative basal diameter of the MH. A moderately reflective lesion is seen in the fovea (asterisk). (Bottom) A vertical scan through the center of the fovea in the direction of the vertical arrow in 2nd row (middle) shows decreased reflectivity of the IS/OS (between red arrowheads) in the fovea. A moderately reflective lesion is seen in the fovea (asterisk). RPE = retinal pigment epithelium.

Figure 7. Adaptive optics scanning laser ophthalmoscopy (AO-SLO) images of an eye with a surgically closed macular hole (the same eye shown in Fig 6). Large dark areas (arrows) are seen on AO-SLO images of the area indicated by the white box in the middle of the 2nd row of Fig 6. The total area of the dark areas is .754 mm^2 . The mean cone density .5 mm from the center of the fovea was 9,375 cones/ mm^2 . Asterisk = center of the fovea. Right (top, bottom): High-magnification views of the areas outlined in white boxes. Scale bar = 100 μm .

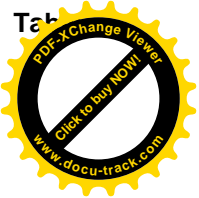


Table 1. Baseline characteristics of eyes with macular holes

Characteristic	Value
Patient age (years), mean \pm 1 SD (range)	67.6 \pm 6.1 (55–82)
Patient gender, no. (%)	
Men	6 (32%)
Women	13 (68%)
Visual acuity, logMAR, mean \pm 1 SD (range)	.584 \pm 0.288 (.155–1.301)
Axial length (mm), mean \pm 1 SD (range)	23.98 \pm 1.30 (22.3–25.9)
Symptom duration (months), mean \pm 1 SD (range)	2.5 \pm 2.44(.5–12.0)
MH stage, no. (%)	
Stage 2	10 (48%)
Stage 3	6 (29%)
Stage 4	5 (24%)
ILM staining, no. (%)	
with TA	8 (38%)
with ICG	13 (62%)
Minimum diameter of MH (μ m), mean \pm 1 SD (range)	303.5 \pm 153.6 (148–726)
Basal diameter of MH (μ m), mean \pm 1 SD (range)	672.7 \pm 323.2 (173–1482)
MH height (μ m), mean \pm 1 SD (range)	376.2 \pm 107.0 (160–532)
IS/OS decreased reflectivity size (μ m), mean \pm 1 SD (range)	1447.8 \pm 894.6 (261–2514)
(reflectivity decreased \geq 2SD)	
OS defect in the fluid cuff, no. (%)	7 (33%)

SD = standard deviation, log MAR = logarithm of minimal angle of resolution, MH = macular hole, ILM = internal limiting membrane, TA = triamcinolone acetonide, ICG = indocyanine green, IS/OS = junction of the photoreceptor inner and outer segment layers, OS = outer segment



Table 2. Comparison of pre- and postoperative characteristics of eyes with macular holes with those of normal eyes

Characteristic	Postoperative Value (MH patients)	Preoperative Value (MH patients)	Normal Eyes
Visual acuity, logMAR, mean \pm 1 SD (range)	.225 \pm .326 (-.079–1.000)	$P < 0.001^*$	-.127 \pm .07 $P < .001^\dagger$
Foveal sensitivity (dB), mean \pm 1 SD (range)	14.0 \pm 4.3	N/A	19.5 \pm .7 $P < .001^\dagger$
Thickness of ONL at the foveal center (μm), mean \pm 1 SD (range)	97.8 \pm 39.0 (37–197)	N/A	122.1 \pm 23.3 $P = .038^\dagger$
Thickness of inner and outer segments at the foveal center (μm), mean \pm 1 SD (range)	67.0 \pm 23.2 (21–92)	N/A	86.0 \pm 5.6 $P = .002^\dagger$
IS/OS decreased reflectivity size (μm), mean \pm 1 SD (range) (reflectivity decreased $\geq 2\text{SD}$)	104.2 \pm 150.9 (0–554)	$P < 0.001^*$	0
Cone density .5 mm from the foveal center (cones/ mm^2), mean \pm 1 SD (range)	19,650 \pm 10,970 (3,182–43,198)	N/A	31,775 \pm 11,418 $P = .003^\dagger$
Dark area within cone mosaic (mm^2), mean \pm 1 SD (range)	.203 \pm .222 (.004–.754)	N/A	0
Moderately reflective foveal lesion, no. (%)	7 (33%)	N/A	0

*paired *t*-test, † Student *t*-test

N/A = not present/not measured; SD = standard deviation, log MAR = logarithm of minimal angle of resolution, ONL = outer nuclear layer, IS/OS = photoreceptor inner and outer segment junction

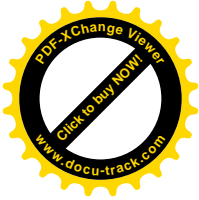
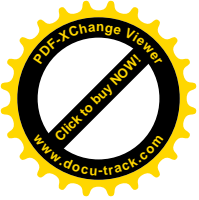


Table 3. Correlation between cone density/dark area and both pre- and postoperative characteristics of eyes with macular holes

Characteristic	Cone density		Cone loss (Dark) area	
	<i>R</i>	<i>P</i> -value	<i>R</i>	<i>P</i> -value
Preoperative				
Patient age	-.496	.211	.206	.369
Visual acuity, logMAR	-.490	.024	.422	.057
Axial length	.391	.121	-.458	.064
Symptom duration	-.342	.129	.731	<.001
Minimum diameter of MH	-.224	.387	.194	.456
Basal diameter of MH	-.178	.494	.258	.317
MH height	-.083	.752	.106	.685
IS/OS decreased reflectivity size	-.353	.151	-.130	.960
Postoperative				
Visual acuity, logMAR	-.742	<.001	.613	.003
Mean foveal sensitivity	.812	<.001	-.651	.006
Thickness of ONL at the foveal center	.004	.985	-.048	.835
Thickness of inner and outer segments at the foveal center	.530	.014	-.444	.044
IS/OS decreased reflectivity size	-.321	.156	.531	.013

log MAR = logarithm of minimal angle of resolution, MH = macular hole, IS/OS = photoreceptor inner and outer segment junction, ONL = outer nuclear layer

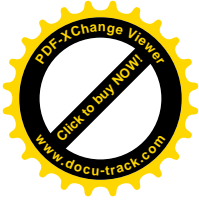


Table 4. Relationship between cone density/dark area and pre-, intra-, and postoperative characteristics of eyes with macular hole

Characteristic		Cone density (cones/mm ²)	P value*	Cone loss (Dark) area (mm ²)	P value*
Preoperative					
Patient sex	Men	21,799 ± 11,095	.583	.098 ± .111	.074
	Women	18,790 ± 11,188		.245 ± .244	
MH stage	2	17,059 ± 10,857	.314	.157 ± .195	.284
	3, 4	22,005 ± 11,035		.264 ± .251	
OS defect in fluid cuff	-	21,913 ± 9,571	.018	.101 ± .133	.001
	+	12,083 ± 6,899		.410 ± .232	
Intraoperative					
ILM staining agent	TA	24,671 ± 12,890	.144	.182 ± .266	.743
	ICG	16,560 ± 8,746		.216 ± .201	
Postoperative					
Moderately reflective foveal lesion	-	24,870 ± 9,463	<.001	.021 ± .016	.001
	+	9,210 ± 4,050		.276 ± .224	

*Student *t*-test

MH = macular hole; IS/OS = photoreceptor inner and outer segment junction, ILM = internal limiting membrane, TA = triamcinolone acetate, ICG = indocyanine green, ONL = outer nuclear layer

